Numerical evaluation of head losses in plate and bar heat exchangers

M Grespan[1,3], A Leonforte[1], M Cavazzuti[1], L Calò[1,2] and D Angeli[3]

[1] DISMI - Dipartimento di Scienze e Metodi dell'Ingegneria, Università di Modena e Reggio Emilia, Via Amendola 2, Pad. Buccola, 42122 Reggio Emilia (Italy)

E-mail: mattia.grespan@unimore.it

[2] VEMA Industries S.p.A., Via Guido Rossa 8, 43058 Sorbolo (Italy)

E-mail: luigi.calo@vema-industries.com

[3] Centro Interdipartimentale EN&TECH, Piazzale Europa 1, 42124 Reggio Emilia (Italy)

E-mail: diego.angeli@unimore.it

Abstract. A numerical model of the internal flow of an air-oil heat exchanger is developed, with the aim of assessing the total head losses, and the single contributions given by the main heat exchanger parts, namely the inlet and outlet manifolds and internal channels. The internal channels are characterized by an offset strip fin design, which is extensively discussed in the literature. Separate CFD analyses are carried out on the single fins, in the hypothesis of fully-developed flow, to determine heat transfer and friction characteristics at multiple flow regimes; the results are compared with the literature, and they are employed to construct suitable correlations, for the friction factor and Nusselt number. In the overall heat exchanger model the internal channels are then replaced by porous regions, to reduce grid size and complexity; the equivalent porosity model is calibrated on the basis of the aforementioned correlations for the single fin. Finally, numerical results are compared with available experimental data, for different values of the flow rate, showing a remarkable agreement, thus corroborating the validity of the proposed numerical approach.

Keywords: plate fin, heat exchanger, CFD, head losses, offset strip fins, porous medium model

1. Introduction

Compact air-cooled heat exchangers are extensively used in automotive, agricultural and construction industries. Among the various construction layouts, the aluminum plate and bar (often referred to as PFHE or plate and fin heat exchangers) ensures remarkable resistance against mechanical and thermal loads, and excellent heat transfer performance. In PFHE, offset-strip fins (OSFs) are widely used to enhance heat transfer. Many studies have been conducted on this kind of fins, and several authors proposed correlations for the friction and Colburn factors on the basis of the geometry, Reynolds

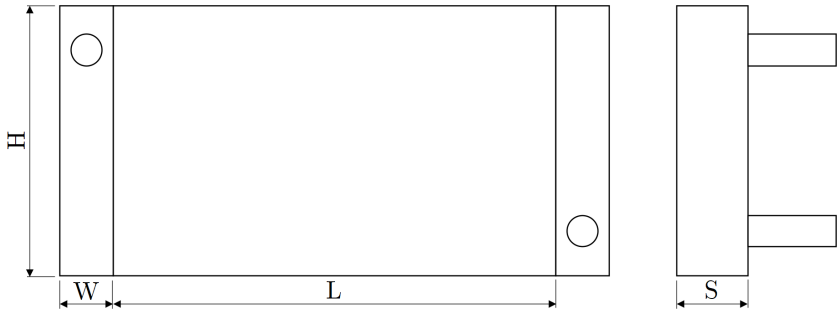

Figure 1. External geometry of the considered heat exchangers.

and Prandtl numbers [1–3]. However, data related to fluids with high Pr values is scarce, and previously conducted studies on the overall friction losses do not include hydraulic oil as working fluid [4–9]. Hence, the accurate prediction of heat transfer and pressure drop in OSFs remains difficult, because of the large number of geometrical parameters involved and different working fluids. The aim of this and future works is to develop an effective numerical tool to evaluate and possibly optimize the performance of PFHE oil coolers featuring offset-strip fins. The model is validated by comparing the results with experimental data.

2. Materials and methods

2.1. Case study

Three air-oil coolers are examined in the present work, these are identified by their thickness $S = 80$, 94 and 113 mm. The height and width of the manifolds are denoted by H and W, respectively. The geometry of the internal channels is defined by the channel height h_{ch}, the pitch x and offset length l. The length of a channel layer is identified by L and the number of ducts is N_{ch}. Table 1 reports the relevant dimensions for all three configurations, as well as providing an identification for future reference. Figure 1 shows a simple drawing of the geometry of the considered coolers.
It is assumed that heat transfer takes place only in the internal channels; hence, the manifolds are considered adiabatic. For the calculation of head losses the contributions of both manifolds and internal tubes are considered instead. With the aim of reducing model complexity and computational effort, the internal channels are analyzed separately, by developing a numerical model for a single fin, to determine the Nusselt

Table 1. Geometrical parameters of the considered air-oil coolers.

ID	S [mm]	H [mm]	W [mm]	L [mm]	h_{ch} [mm]	x [mm]	l [mm]	N_{ch}
S80	80	304	60	500	3	1.5	5	20
S94	94	309	60	500	3	1.5	5	21
S113	113	305	60	500	3	1.5	5	20

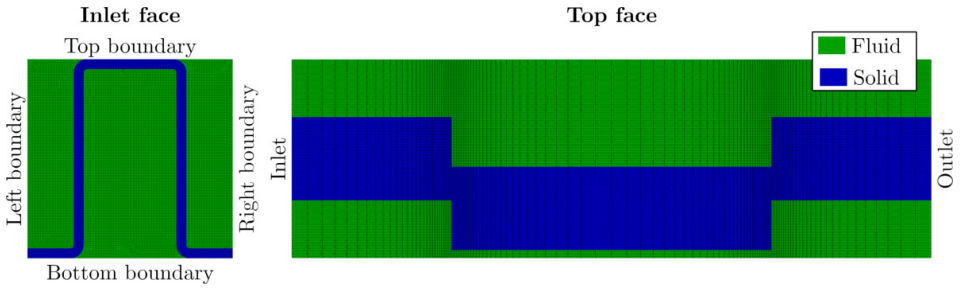

Figure 2. Computational mesh of the single fin: selected views.

number and equivalent friction factor for several flow regimes. This process allows for the obtainment of suitable correlations to extend the results to the entire channel. The complete heat exchanger is analyzed by building up a CFD model, in which the inlet and outlet manifolds are connected by porous regions, that represent the internal channels. The equivalent porosity model is calibrated on the basis of the aforementioned friction factor correlation. Thus, the total head losses can be computed without the need for computationally intensive calculations.

2.2. Single fin model

The single fin is modelled by considering the smallest unit geometry, which repeats itself along the width and length of the duct. The fin is assumed to be placed away from the inlet and outlet sections; under this hypothesis the flow can be considered fully developed. The flow is assumed steady-state and incompressible, as fluid velocity is always a fraction of the speed of sound, which is 1700 m/s for mineral oil. The fluid flow at different Reynolds numbers is determined by solving the momentum, continuity and energy equations. The range of Re-values encompassed (15 - 300) is such that the flow can be considered as laminar.

$$\begin{cases} \nabla \cdot (\vec{v} \otimes \vec{v}) = -\dfrac{1}{\rho} \nabla p + \nu \nabla^2 \vec{v} + \vec{g} \\ \nabla \cdot \vec{v} = 0 \\ \nabla \cdot (\rho \vec{v} h) + \nabla \cdot \left(\rho \vec{v} \dfrac{|\vec{v}|^2}{2} \right) = -\nabla \cdot \vec{q} + \nabla \cdot (\vec{\tau} \cdot \vec{v}) + \rho \vec{g} \cdot \vec{v} \end{cases} \tag{1}$$

The temperature field in the solid regions is determined by solving the conduction equation.

$$\nabla \cdot (\alpha \nabla h) = 0 \tag{2}$$

The governing equations are solved numerically, by applying a Finite Volume numerical method; the algebraic equations are solved by using the SIMPLE algorithm. The domain is discretized with a hybrid mesh, as shown in figure 2. To account for the periodicity of the channel geometry in the flow direction velocity and temperature distributions at the inlet section are mapped from the outlet face, while maintaining fixed integral average values, and a zero gradient condition is imposed on the pressure field. At the

outlet section the pressure is set to a reference value, while a zero gradient condition is applied to velocity and temperature. Periodic conditions are enforced along the spanwise direction. At the top and bottom surfaces the temperature gradient is set to an arbitrary non-zero value, to impose an exiting heat flux. At walls, no-slip conditions are applied to the velocity field and a zero pressure gradient is imposed. Finally, continuity of temperature and heat flux is enforced at all fluid-solid interfaces.

The equivalent friction factor of the single fin is defined here as:

$$f = \frac{h_{\mathrm{ch}}\,(\bar{p}_i - \bar{p}_o)}{l\,\rho\,\bar{u}_i^2} \tag{3}$$

where overbars indicate integral mean field values over the inlet (i) and outlet (o) surfaces. The Nusselt number is calculated by considering the average fluid bulk temperature between the inlet and outlet surfaces $\bar{T}_b = 0.5\,(T_{b\,i} + T_{b\,o})$. The wall temperature $\bar{T}_w$ is the integral mean of the temperature field over the heat exchange area A_{ref}, which is made up of the fluid-solid interface and the top and bottom boundaries.

$$\mathrm{Nu} = \frac{\dot{\mathrm{Q}}\,\mathrm{h_{ch}}}{\lambda\,\mathrm{A_{ref}}\,(\bar{\mathrm{T}}_{\mathrm{b}} - \bar{\mathrm{T}}_{\mathrm{w}})} \tag{4}$$

2.3. Overall model

The overall heat exchanger model is formed by the inlet and outlet manifolds, along with the porous regions that represent the internal channels. The incompressible oil flow is determined by solving the steady-state RANS equations.

$$\begin{cases} \nabla \cdot (\ \vec{v} \otimes \vec{v}\ ) = -\dfrac{1}{\rho}\,\nabla p\ + \nabla \cdot [\ (\nu + \nu_t)\,\nabla \vec{v}\ ] - S_{\mathrm{m}} \\ \nabla \cdot \vec{v} = 0 \end{cases} \tag{5}$$

Where S_{m} is a momentum sink term, that is non-zero only in the porous regions:

$$S_{\mathrm{m}} = \left(\nu \vec{D} + \frac{1}{2}\,\mathrm{tr}(\vec{v} \cdot I)\,\vec{F}\right)\vec{v} \tag{6}$$

in (6) the vectors $\vec{D}$ and $\vec{F}$ define the momentum loss given by the porous regions, and they are determined from the single fin friction factor correlation (see equation (7), which will be presented later). The equations are solved numerically, with a Finite Volume approach. The heat exchanger domain is discretized with a hybrid mesh, which is shown in figure 3. At the inlet a constant velocity value is imposed, and a zero gradient boundary condition is assigned to the pressure field. At the outlet the surface mean pressure is set to a reference value; a zero gradient is imposed to the velocity field. At the walls a no-slip condition is enforced. The discretized equations are solved with the SIMPLE algorithm. The pressure drops relative to the manifolds and internal channels are calculated considering the integral mean of the pressure field on the boundary faces of these components. Four runs are executed for each heat exchanger geometry, one for each flow rate value experimentally tested.

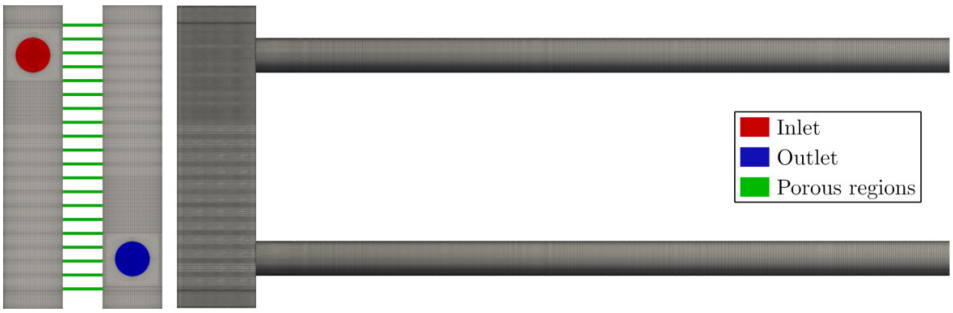

Figure 3. Sample mesh of the overall model.

2.4. Experimental apparatus and procedures

The heat exchangers have been tested in a small wind tunnel, powered by a radial fan. The air mass flow rate is measured with a V-Cone flow meter. The pressure drop on the oil side is measured by differential pressure transducers. The oil flow rate is measured with an impeller device, and Pt100 sensors are used for temperature. Air temperature is measured with type K thermocouples. Thermal tests were performed considering four air and oil flow rates. The oil flow rate varies between 60 and 150 l/min, while the air flow rate ranges between 2600 and 6500 kg/h. In the following section, the different flow rates will be addressed by means of the respective Reynolds number value, based on the diameter of the inlet pipe.

3. Results

3.1. Single fin

Figure 4 shows a cross-section of the velocity field, taken at the fin half height. The development of the boundary layers on the walls is clearly shown. At the trailing edge of each wall, wakes are formed due to flow separation. The values of Nusselt number and equivalent friction factor, resulting from each CFD analysis, are used to determine correlations, as a function of the Reynolds number only.

$$f = 195.3\,\mathrm{Re}^{-0.9761} + 0.1561 \tag{7}$$

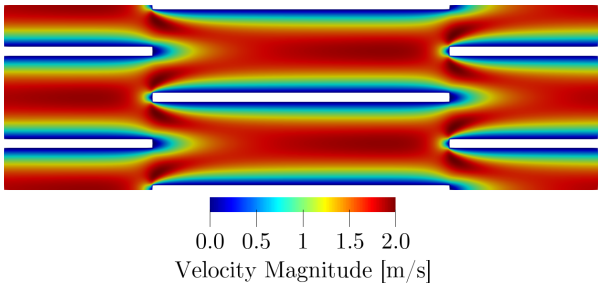

Figure 4. Single fin: colormap of velocity magnitude along a longitudinal cross-section, as obtained by CFD.

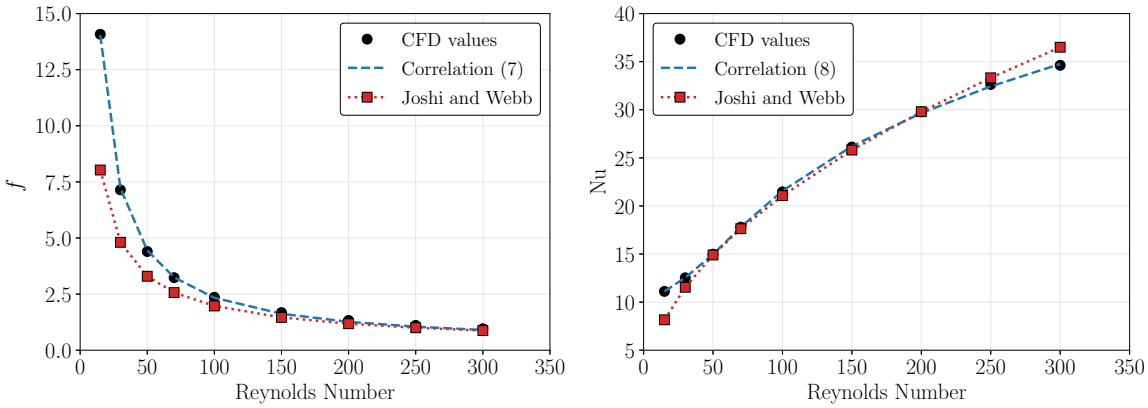

(a) (b)

Figure 5. Single fin: friction factor (a) and Nusselt number (b) data, as compared with the literature.

$$\mathrm{Nu} = \begin{cases} 0.0205\,\mathrm{Re}^{1.392} + 10.22 & \text{for } \mathrm{Re} \leq 70 \\ 41.74\,\mathrm{Re}^{0.1398} - 57.89 & \text{for } 70 < \mathrm{Re} \leq 300 \end{cases} \tag{8}$$

In figure 5 the numerical results are compared with Nu and f values obtained from the correlations presented by Joshi and Webb [10]. At low Reynolds numbers the difference is noticeable between the friction factor estimated by CFD and the data presented by Joshi and Webb. This difference justifies the present analysis, since oil flow in the internal channels typically occurs at very low Reynolds numbers. A very good agreement is found instead for the Nusselt number values over the whole Reynolds number range, except for a significant deviation occurring for the minimum and maximum Re-values considered.

3.2. Overall model

Figure 6 shows cross-sections of the velocity field at Re = 2200, related to the 80 mm wide heat exchanger; the slices are taken at the symmetry planes of the inlet and outlet ducts, respectively. At the inlet the fluid enters the manifold at high speed and impinges the wall opposite to the inlet section. As the fluid is deviated along the wall two large vortex structures are generated. In the outlet manifold velocity is much more uniform, while it increases in proximity of the outlet duct, and two recirculation regions are formed in the entrance section of the tube. These vortices effectively restrict the outflow section, leading to major head losses. To understand how each component of the exchanger contributes to the total losses, the pressure drops across the manifolds and internal channels are expressed as a fraction of the overall pressure drop, for each inlet Reynolds number. As it can be seen in figure 7a, at high Reynolds numbers the specific loss related to the outlet manifold becomes more relevant, weighing as much as 14% of the total loss, while the contribution of the channels decreases. On the other hand, in the considered Re-range the inlet weight of the pressure loss remains

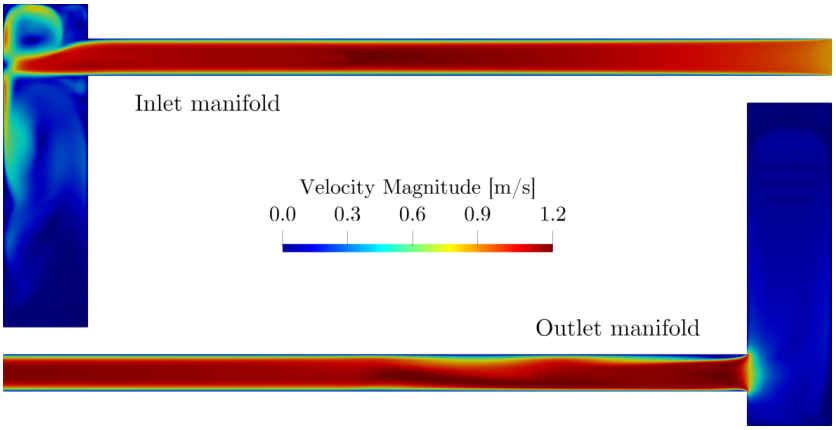

Figure 6. Overall model: colormaps of velocity magnitude along vertical cross-sections at the inlet and outlet manifolds, as obtained by CFD.

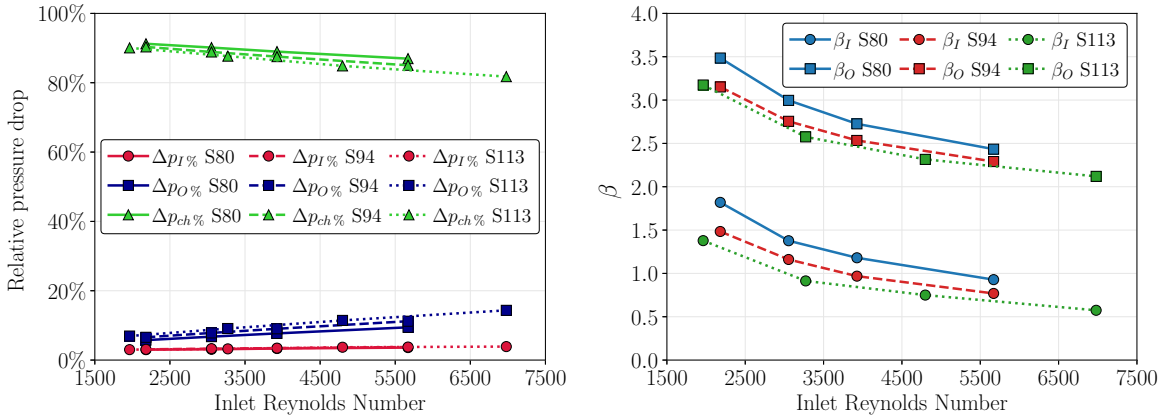

Figure 7. Overall model: relative pressure drop distribution (a) and concentrated loss coefficients (b).

constant at 3%. Concentrated loss coefficients related to the inlet and outlet manifolds are calculated for each inlet Reynolds number (figure 7b). As expected, the curves decrease with the Reynolds number, and as the cooler width decreases both inlet and outlet loss coefficients increase. To verify the validity of the numerical model the total head losses Δp_T are compared with experimental values for each inlet Reynolds number (figure 8a). The maximum difference between numerical and experimental results is 16%, and in the majority of the tested points the difference is less than 10%. The accuracy of these results is remarkable, considering that the numerical model is purely derived from nominal geometric data, and that shape imperfections, which are inevitable in the manufacturing process, were not considered. The thermal performance is verified by calculating the heat exchanged by the S94 cooler for different values of the air mass flow rate (figure 8b). Details of the thermal model are omitted here for brevity, it is only mentioned that the $\varepsilon - NTU$ method is employed, and the conductive resistance

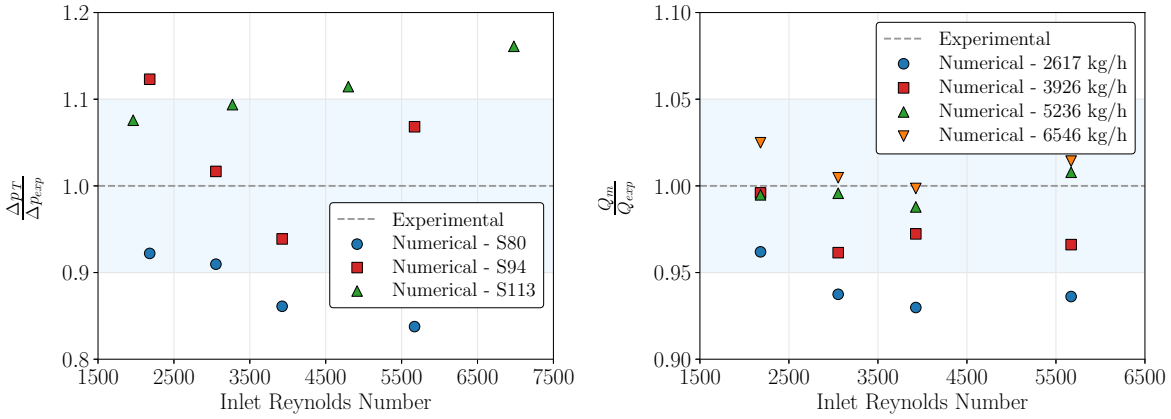

Figure 8. Overall model: comparison with experimental data in terms of head losses (a) and heat transfer rates (b).

of the fins is neglected. The maximum deviation between numerical and experimental results is 7%, and for most of the cases the difference is less than 5%.

4. Conclusions

A numerical model for the internal flow of plate and bar heat exchangers has been developed. The internal fins, of offset-strip design, were analyzed separately to determine their heat transfer and friction characteristics. These results were used to develop an overall heat exchanger model, which was then applied to three air-oil cooler geometries. The computed head losses and heat transfer rates were in good agreement with experimental results. Future research activity will be focused on different internal fluids and fin geometries, with the aim of generalizing the model.

References

[1] Hu S and Herold K E 1995 *International Journal of Heat and Mass Transfer* **38** 1053–1061
[2] Peng H and Ling X 2008 *Experimental Thermal and Fluid Science* **32** 1039–1048
[3] Manglik R M and Bergles A E 1995 *Experimental Thermal and Fluid Science* **10** 171–180 aerospace Heat Exchanger Technology
[4] Chiou J P 1978 *J. Heat Transfer.* **100** 580–587
[5] Bassiouny M and Martin H 1984 *Chemical Engineering Science* **39** 693–700
[6] Ranganayakulu C and Seetharamu K 1999 *International Communications in Heat and Mass Transfer* **26** 669–678
[7] Jiao A, Zhang R and Jeong S 2003 *Applied Thermal Engineering* **23** 1235–1246
[8] Zhang Z and Li Y 2003 *Cryogenics* **43** 673–678
[9] Wang C C, Yang K S, Tsai J S and Chen I Y 2011 *Applied Thermal Engineering* **31** 3226–3234
[10] Joshi H M and Webb R L 1987 *International Journal of Heat and Mass Transfer* **30** 69–84